Published in final edited form as:
Soft Matter. 2013 December 7; 9(45): 10877–10884. doi:10.1039/C3SM51829A.

Monolayer spontaneous curvature of raft-forming membrane lipids

Benjamin Kollmitzer[a], **Peter Heftberger**[a], **Michael Rappolt**[b,c], and **Georg Pabst**[a]

[a]Institute of Molecular Biosciences, Biophysics Division, University of Graz, Austria. Georg.Pabst@uni-graz.at; Fax: +43 316 4120-390; Tel: +43 316 4120-342

[b]Institute of Inorganic Chemistry, Graz University of Technology, Austria

[c]School of Food Science and Nutrition, University of Leeds, UK

Abstract

Monolayer spontaneous curvatures for cholesterol, DOPE, POPE, DOPC, DPPC, DSPC, POPC, SOPC, and egg sphingomyelin were obtained using small-angle X-ray scattering (SAXS) on inverted hexagonal phases (H_{II}). Spontaneous curvatures of bilayer forming lipids were estimated by adding controlled amounts to a H_{II} forming template following previously established protocols. Spontaneous curvatures of both phosphatidylethanolamines and cholesterol were found to be at least a factor of two more negative than those of phosphatidylcholines, whose J_0 values are closer to zero. Interestingly, a significant positive J_0 value was retrieved for DPPC. We further determined the temperature dependence of the spontaneous curvatures $J_0(T)$ in the range from 15 to 55 °C, resulting in a quite narrow distribution of −1 to -3×10^{-3} $(\text{nm °C})^{-1}$ for most investigated lipids. The data allowed us to estimate the monolayer spontaneous curvatures of ternary lipid mixtures showing liquid ordered/liquid disordered phase coexistence. We report spontaneous curvature phase diagrams for DSPC/DOPC/Chol, DPPC/DOPC/Chol and SM/POPC/Chol and discuss effects on protein insertion and line tension.

1 Introduction

Curvature is an essential ingredient in a cell's life and occurs most visibly during membrane fusion and fission processes, *e.g.* exocytosis and endocytosis, or when a cell is attacked by an enveloped virus.[1] Such events may be induced by proteins, but are also known to depend strongly on the molecular properties of the constituent membrane lipids.[2] For instance membrane fusion can take place in the absence of proteins.[3] Lipid-driven membrane curvature may result *e.g.* from unequally distributed lipids of the same type in the opposing membrane leaflets or from asymmetric distributions of lipids with different molecular shapes due to their different intrinsic curvatures.[4-9]

In general, lipids with molecular shapes different from cylinders will form monolayers that either curve away or towards the polar/apolar interface.[10] In planar membranes, however, such monolayers are forced into a flat topology, where they lie back-to-back – in order to avoid energetically unfavorable voids – leading to significant curvature elastic stress that is stored within the membrane. This elastic stress may have several functional consequences for membranes and can be viewed as a hidden dimension of membrane curvature. Of particular interest is the role of intrinsic/spontaneous curvature in coupling to protein

Europe PMC Funders Author Manuscripts

function[11-18] and in determining the line tension of lipid domains mimicking membrane rafts.[19,20]

As per definition the spontaneous curvature $J_0 = 0$ for cylindrically formed lipids, $J_0 < 0$ for lipids with tail regions of bigger lateral cross-section than the headgroups and *vice versa* for $J_0 > 0$. For example, lipids with a negative spontaneous curvature are prone to form non-planar structures like inverted hexagonal phases H_{II}. More precisely the radius of curvature of an unstressed monolayer at its neutral plane equals $1/J_0$.[21,22] The neutral plane is defined as the position at which bending and stretching modes are decoupled, *i.e.* bending and stretching deformations proceed independently from each other.[23] A second, frequently quoted surface within the monolayer of amphiphiles is the pivotal plane, which occurs where the molecular area does not change upon deformation. Pioneered by the groups of Rand and Gruner during the late 80s and the 90s, the position of this surface and consequently the spontaneous curvature at the pivotal plane J_{0p} have been determined to high accuracy for a couple of membrane lipids,[21,24-30] for review see ref. 31. The basic idea of these experiments is to use H_{II} phases, where the lipid monolayers expose their intrinsic curvature within the individual rods and to determine the pivotal plane by bending and compressing the rods either by gravimetric dehydration or application of osmotic pressure, while measuring the crystalline lattice *via* X-ray scattering. For a limited number of lipids the neutral plane has been estimated from the pivotal surface using area compressibility and bending rigidity data.[21,23,32]

In the present work we determine J_0 under stress-free conditions by locating the neutral plane from electron density maps of H_{II} phases. In particular we focus on spontaneous curvature data of lipids which are involved in the formation of membrane rafts. Such data are especially of need for calculating protein partitioning in diverse lipid environments[11-18] or to estimate the line-tension of lipid domains.[19,20] Additionally, the temperature dependence of spontaneous curvature is still barely investigated. We intend to bridge this gap by determining J_0 for cholesterol, DOPC, DPPC, DSPC, POPC, SOPC and egg sphingomyelin within a DOPE matrix from 15 to 55 °C and for POPE at 37 and 55 °C.

2 Materials and methods

2.1 Sample preparation

Cholesterol (Chol), 1,2-dioleoyl-*sn-glycero*-3-phosphocholine (DOPC), 1,2-dioleoyl-*sn-glycero*-3-phosphoethanolamine (DOPE), 1,2-dipalmitoyl-*sn-glycero*-3-phosphocholine (DPPC), 1,2-distearoyl-*sn-glycero*-3-phosphocholine (DSPC), 1-palmitoyl-2-oleoyl-*sn-glycero*-3-phosphocholine (POPC), 1-stearoyl-2-oleoyl-*sn-glycero*-3-phosphocholine (SOPC), and chicken egg sphingomyelin (eggSM) were purchased from Avanti Polar Lipids, Inc., Alabaster, AL, USA and used without further purification. 9-*cis*-Tricosene was obtained from Sigma-Aldrich, Austria.

After weighing, lipids were dissolved in chloroform-methanol 2: 1 at a concentration of 10 mg ml^{-1}. These lipid stock solutions were mixed in glass vials, 12 wt% tricosene was added and the organic solvent was evaporated under a gentle nitrogen stream. To remove the remaining solvent, the samples were placed in a vacuum overnight. 18 MΩ cm^{-1} water (UHQ PS, USF Elga, Wycombe, UK) was added to 20 μl mg^{-1} lipid and the mixtures with repeated freeze-thaw cycles fully hydrated. The samples were then protected against oxidation with argon, the vials closed and taped, and stored at 4 °C for 6-7 days until the measurement.

2.2 X-ray measurements

Small-angle X-ray scattering (SAXS) was performed at the Austrian SAXS beamline at ELETTRA, Trieste.[33,34] A mar300 Image Plate 2D detector from Marresearch, Norderstedt, Germany was used covering a q-range from 0.2–6.1 nm^{-1} and calibrated with silver-behenate ($CH_3(CH_2)_{20}COOAg$) with a d-spacing of 5.838 nm.[35] Sample temperatures were controlled with a bath thermostat from Huber, Offenburg, Germany to a precision of ±0.1 °C. The samples were equilibrated for 10 min at given temperatures before exposure. The exposure time was set to 30 s.

2.3 X-ray data analysis

Image integration was performed with FIT2D[36,37] and cross-checked with MATLAB®.[38] For further data analysis, homemade MATLAB scripts were used and their function verified with FIT2D,[39] IDL®,[40] and IGOR Pro®.[41]

Standard procedures were used to determine the lattice parameters and calculate electron-density maps of the H_{II} (for further details, see S1 of the ESI). In brief, we applied Lorentzians and additive linear background estimators to fit the Bragg peaks. Typically 5-7 peaks were discernible in the patterns, although for higher temperatures and some samples only three or four peaks could be detected. This was considered in the uncertainty estimations.

The lattice parameter a was determined *via* the reflection law, taking into account the information from all Lorentzians. Fourier synthesis yielded the electron density $\rho(\vec{r})$ in real-space, with the phasing condition (+ −− + + + + + −) known from the literature for DOPE-rich, fully hydrated H_{II} phases.[42-44] Other phase combinations were tested, but yielded electron densities incompatible with the known structure.

2.4 Spontaneous curvature estimation

2.4.1 Finding the neutral plane—Instead of bending and compressing lipid monolayers with osmotic pressures to determine the position $R_0 = 1/J_0$ of the neutral plane,[21] we applied the following procedure, assuming that the neutral plane coincides with the glycerol backbone of phospholipids. This assumption is supported by bending/compression experiments, which always found the pivotal plane to be close to the glycerol backbone of lipid molecules, but slightly within the hydrocarbon region,[21,24-30,44,45] while the neutral plane was estimated to be closer to the backbone.[21,32] The proximity of both surfaces to the backbone can be rationalized by the high rigidity in this region.[22] In general, the positions of the neutral and pivotal planes differ by less than 10% and can even coincide when monolayers are bent in the absence of compression.[21,22]

We first locate the position R_p of the lipid headgroup by fitting a Gaussian to a radial section of the electron density map in a region of ~1 nm around the maximum value (see S1 in the ESI for further details). Then, the neutral surface is simply given by $R_0 = R_p + d_{H1}$, where d_{H1} is the distance between the headgroup and the glycerol backbone. Using a joint refinement of X-ray and neutron data on lamellar phases, Kučerka and coworkers reported high-resolution structural data for a series of phospholipids.[46-49] The reported d_{H1} values range between 0.37 and 0.50 nm at temperatures from 20 to 50 °C. We apply the average of these values for our R_0 calculations $d_{H1} = (0.44 \pm 0.05)$ nm. To test the applicability of this procedure, we compare $J_0 = (-0.387 \pm 0.011)$ nm^{-1} retrieved from the present analysis for DOPE at 25 °C with $J_0 = (-0.367 \pm 0.010)$ nm^{-1} estimated from measurements of the pivotal surface.[21] A small difference is expected due to the presence of tricosene in the present experiments in order to reduce packing frustration (see Section 2.4.2) as compared to the measurements performed by Leikin *et al.*[21]

We also attempted to derive J_0 from the width σ_p of the Gaussian fitted to the headgroup region of the radial electron density profiles, *i.e.* $R_0 = R_p + \sigma_p$. However, the resolution of the electron density maps was too poor for some lipid mixtures, yielding $\sigma_p > 0.7$ nm and hence unrealistic locations of the glycerol backbone.

2.4.2 Relaxation of hexagonal packing frustration—Stress free monolayers, which are necessary for measuring the monolayer spontaneous curvature J_0, are usually obtained by adding free alkanes or alkenes to inverted hexagonal phases H_{II}.[26,30,50,51] By taking up the interstitial spaces, they can reduce the frustration of packing circular objects in a hexagonal manner. This effect is impressively seen for POPE, which forms in the absence of any additive a H_{II} phase only above 74 °C.[52] Addition of tricosene reduced the frustration to such an amount that already at 37 °C the H_{II} phase was preferred. The total tricosene content of all our samples was 12 wt%. The value was obtained from a test series of varying tricosene concentrations and is close to the 10 wt% used in ref. 45.

2.4.3 Spontaneous curvature of bilayer-forming lipids—Because monolayer J_0 is not accessible in bilayers due to symmetry constraints, bilayer-forming lipids have to be incorporated into other structures, see Fig. 1. Usually H_{II} phases (we use the H_{II} forming lipid DOPE) are used as templates by mixing the lipid of interest ("guest") with a H_{II}-forming "host" lipid.[17,26,29,45,53] As long as both lipids mix well, the guest lipid can be expected to modify the curvature of the mixture linearly with respect to its concentration χ[54-57]

$$J_0^{\mathrm{mix}} = \chi J_0^{\mathrm{guest}} + (1-\chi) J_0^{\mathrm{host}} \quad (1)$$

and extrapolation towards 100% gives the spontaneous curvature of the guest lipid.[21] A more sophisticated description of spontaneous curvature calculations for lipid mixtures has been reported.[58] However, the experimental determination of several model parameters in this theory remains unclear and experiments seem to contradict with these calculations.[59]

All bilayer-forming lipids were measured at concentrations of 10, 20, 30, 40 and 50 mol% in DOPE. The extrapolation according to eqn (1) was performed using all concentrations below a critical value χ_{crit}, at which:

- immiscibility was directly observed because non-hexagonal Bragg peaks were visible,
- eqn (1) did not obviously hold anymore, or
- the lattice parameter *a* did not change smoothly with χ.

Entropic contributions get more pronounced at higher temperatures, which generally leads to improved miscibilities. Accordingly, we observed a monotonic increase of χ_{crit} with *T* for all samples. An example of the occurrence of non-hexagonal peaks is given in Fig. 2.

Good miscibility was observed for Chol and all unsaturated lipids. For saturated lipids χ_{crit} was not equally satisfactory, but improved above the melting transition of the guest lipid with the exception of eggSM, where only 10 mol% could be incorporated into the DOPE matrix at all temperatures. The number of useful data points (where $\chi < \chi_{crit}$) is taken into account for determining the uncertainty of the resulting J_0. Extrapolation plots and χ_{crit} (*T*) for all lipids are reported in S4 of the ESI.

2.4.4 Temperature dependence—We performed synchrotron SAXS measurements at 10 °C intervals from 15–55 °C for all lipids except POPE to quantify the spontaneous

curvature's temperature dependence $J_0(T)$. The results could be well described within experimental errors by a straight line

$$J_0(T) = k(T - T_m) + J_0^m \quad (2)$$

$$\Delta J_0(T) = \sqrt{(\Delta k)^2 (T - T^m)^2 + (\Delta J_0^m)^2} \quad (3)$$

where we introduced a mean temperature T^m = 35 °C, the coefficient of thermal curvature change k, and J_0^m the spontaneous curvature at T^m, while ΔX denotes the uncertainty of the quantity X. POPE was measured at 37 and 55 °C. Note that POPE forms a H_{II} phase at these temperatures only in the presence of an agent such as tricosene that relaxes the packing frustration. Fits of $J_0(T)$ in comparison to literature data are plotted in S5 of the ESI.

3 Results

Chol, DOPC, DPPC, DSPC, POPC, SOPC and eggSM were mixed with DOPE and measured as detailed in the previous section. The pure lipids' monolayer spontaneous curvatures for each temperature were obtained by eqn (1) (data in S4 of the ESI). Linear fits of the temperature dependence of J_0 yielded the values listed in Table 1 (fits in S5 of the ESI). By inserting these parameters in eqn (2) and (3), J_0 and its uncertainty are readily available for any temperature from 15 to 55 °C.

POPE was measured with 12 wt% tricosene and excess water at 37 and 55 °C in the absence of DOPE. The slope and offset of a straight line through the two points following eqn (2) with T^m = 37 °C are given in Table 1.

Fig. 3 compares our results for cholesterol with literature data.‡ Although it seems like the literature data has a positive slope of $J_0(T)$, this is probably a coincidence and due to the uncorrelated experiments in different lipid host systems. Generally, one would expect the chains to be more flexible and therefore also occupy more space at higher temperature, corresponding to a more negative spontaneous curvature. This behavior corresponds to $k < 0$, which is the case for all lipids except for eggSM. This is most likely an artifact due to the limited miscibility of eggSM with DOPE. The limited miscibility also affected other saturated lipids leading to significant experimental uncertainties in k. The overall k varied in a quite narrow window from −1 to -3.5×10^{-3} (nm °C)$^{-1}$, *cf.* Table 1, in good agreement with $k = (-1.7 \pm 0.3) \times 10^{-3}$ (nm °C)$^{-1}$, reported for DOPE at temperatures from 15 to 30 °C.[27]

Interestingly, DPPC is the only bilayer-forming lipid with a significant positive J_0. DSPC, for example, with the same headgroup but longer chains has $J_0 = -0.1$ nm^{-1} at 35 °C. Thus, the headgroup contribution to the molecular shape dominates the cross-sectional area and hence J_0 of DPPC, whereas chain contributions dominate in the case of DSPC. Mismatch in lateral areas of heads and chains is known to cause chain tilt and the ripple phase for saturated phosphatidylcholines in a certain range of chain lengths.[60] Surprisingly, $J_0 \sim -0.1$ nm^{-1} also for eggSM, which similar to PCs has a choline moiety in the headgroup and is predominantly composed of the same hydrocarbons as DPPC. Here the sphingosine backbone of eggSM seems to make the difference by taking up more lateral space than the

‡Reported values for J_{0p}[17,29] were rescaled to J_0 using $J_0 \sim J_{0p}(1 + \beta)$, with $\beta = 0.065 \pm 0.035$ determined in ref. 21. Data reported by Boulgaropoulos et al.[17] were additionally corrected from $J_{0p} = -0.38$ nm^{-1} to −0.43 nm^{-1} prior to the scaling due to a flaw in their data analysis.

glycerol backbone of PCs. A detailed investigation of this effect is, however, beyond the scope of the present work.

4 Discussion

4.1 Monolayer spontaneous curvature of phase separated systems

For known compositions, monolayer spontaneous curvatures of mixtures are readily computable by generalization of eqn (1) to more components, resulting in

$$J_0^{\mathrm{mix}} = \sum_i \chi_i J_0(i) \quad (4)$$

As already mentioned, miscibility is required for the linear additivity of spontaneous curvatures. We assume that this criterion is fulfilled within individual domains of a phase separated system, *i.e.* non-ideal mixing is not considered. Thus if the compositions of coexisting phases are known, eqn (4) can be applied to determine their spontaneous curvatures. In the case of non-ideal mixing, which may occur for example by a preferred location of lipids at the domain boundary, energetic contributions from lipid-lipid interactions and mixing entropies need to be considered (see *e.g.* ref. 58). However, this is beyond the scope of the present paper.

Compositional phase diagrams including tielines have been published recently for ternary lipid mixtures exhibiting liquid disordered (L_d)/liquid ordered (L_o) phase coexistences.[61-63] These mixtures are simple lipid-only models for membrane rafts, complex platforms which are thought to enable cellular communication and material transport.[64] We parameterized the proposed coexistence regions and tieline fields according to the method introduced by Smith and Freed[65] and slightly modified by Heberle *et al.*,[62] whose notation we adopted. Briefly, a given phase coexistence region is approximated *via* a Bézier curve of degree five, while a single variable takes care of the tieline fanning. The parameter $u \in [0, 1]$ identifies a particular tieline, with the critical point (tieline of length 0) at $u = 0$ and the tieline farthest away from the critical point at $u = 1$. More details on this parameterization and the explicit values can be found in S2 of the ESI.

Fig. 4 compares the spontaneous curvatures for coexisting L_o/L_d phases. The mixture POPC/eggSM/Chol behaves as expected, *i.e.* due to the negative intrinsic curvature of cholesterol, the L_o phase, which contains about twice as much cholesterol as L_d domains, exhibits a more negative J_0. Also DOPC/DSPC/Chol shows a similar behaviour, although the measurement uncertainty limits a clear distinction of the spontaneous curvatures of L_o and L_d. For DOPC/DPPC/Chol, however, J_0 of the liquid ordered phase at high values of u is less negative than for the L_d phase, and within the measurement uncertainty it could even be slightly positive. This results from a more positive J_0 of DPPC as compared to DSPC with $J_0 \sim -0.1\ \mathrm{nm}^{-1}$ (Table 1). We note that the quantitative difference between monolayer spontaneous curvatures of L_o and L_d depends on the exact location of the coexistence region and the tieline orientation, which both contain some uncertainties.

It is instructive to consider the effects of these J_0 differences on the insertion probability of simple membrane proteins. Barrel-like transmembrane proteins, which have a thicker cross-section at the center of the bilayer than near the bilayer-water interface, would generally prefer phases with positive spontaneous curvatures, where the effective lipid cross-section at the tail region is smaller than for the headgroup (Fig. 5). In the DOPC/DPPC/Chol case, this simple argument would mean that the L_o phase is more attractive for such proteins. However, a lower-order expansion of the lateral pressure profile already reveals a

Europe PMC Funders Author Manuscripts

dependence of protein partitioning on further elastic parameters, specifically bending elasticities and Gaussian curvature moduli of L_o and L_d.[11,12] The literature suggests furthermore hydrophobic mismatch[66] and disturbance of lipid packing[67,68] as important factors for determining protein-insertion energies in membranes. The treatment of these effects is beyond the scope of the present work.

4.2 Line tension calculation

Another parameter that is affected by J_0 is the line tension γ between two coexisting phases, which influences the size and shape of domains.[69,70] Theory predicts an elastic contribution to γ by the monolayer bending moduli, tilt moduli, and thickness difference of L_o/L_d domains (γ_{el}) and a second term γ_{J0}, which includes contributions from the spontaneous curvatures.[19] In the following paragraphs, we give results for the line tension of ternary and quaternary lipid mixtures and discuss the effect of J_0. Calculation details, lipid compositions of L_o and L_d phases, as well as elastic parameters are given in S3 of the ESI. It is important to note that Helfrich's definition of spontaneous curvature,[71] which has been applied for deriving γ_{J0} in ref. 19, differs from the quantity J_0 which we determine in the present work. However, in the case of linear bending behavior, or for small deviations from a flat monolayer, *i.e.* if the spontaneous curvature is much smaller than the inverse monolayer thickness h, the two values are approximately equal.[22] In S3 of the ESI, we show that indeed $|J_0| < 1/h$ for the following calculations.

Just recently, bending and tilt moduli, as well as structural parameters, have been determined with molecular dynamics (MD) simulations supported by SAXS, for two ternary mixtures showing L_o/L_d phase separation.[72] By combining this information with our new curvature data, we calculate $\gamma = 1.4$ pN for DOPC/DPPC/Chol and $\gamma = 1.6$ pN for DOPC/DSPC/Chol at given L_o/L_d compositions. These values are in the typical range reported from either experiment or theory (see, *e.g.* ref. 73-76). Because of the positive curvature of DPPC, J_0 values for both phases of DOPC/DPPC/Chol are close to zero, leading to vanishing contributions of γ_{J0} to the line tension. For DOPC/DSPC/Chol, however, the L_o and L_d phases feature a negative J_0, leading to $\gamma_{J0} = -1.8$ pN, *i.e.* the line tension between the coexisting domains is decreased due to the contribution of J_0.

The same theory has been applied to rationalize the transition from nanoscopic to microscopic domains, recently reported for the quaternary mixture DOPC/POPC/DSPC/Chol.[77] Starting from nanometer sized domains in POPC/DSPC/Chol, replacing POPC with DOPC has lead to increasing domain sizes, and finally to domains in the micrometer regime for DOPC/DSPC/Chol. Parameterized by the ratio $\rho = \chi_{DOPC}/(\chi_{DOPC} + \chi_{POPC})$, the original calculation of the line tension has explained this behavior; but apart from information on the bilayer thickness only estimated values for the parameters influencing γ were available. By applying bending and tilt moduli from MD simulations,[72] spontaneous curvatures from the current work, and structural information from Heberle *et al.*,[77] we were able to calculate the line tension for $\rho = 1$ and give improved estimations for $\rho < 1$ (Fig. 6). Because of compositional differences for L_o/L_d domains between experiments and MD simulations, the present calculations still rely on considerable assumptions for $\rho < 1$. In general, the change of nanoscopic to microscopic domains is accompanied by an increase of line tension. This agrees well with our results of $\gamma \sim 0.5$ pN for the nanoscopic regime, $\gamma \sim 2.5$ pN for the microscopic regime, and intermediate in between. The contribution of spontaneous curvature to γ stays nearly constant for all compositions, meaning that the transition from nanoscopic to microscopic domains is mainly driven by bilayer thickness differences in this case, in agreement with the conclusions of the original report.[77]

5 Conclusions

By evaluating synchrotron SAXS data of DOPE-rich lipid mixtures in the H_{II} phase, we were able to estimate monolayer spontaneous curvatures J_0 for several biologically relevant phospholipids, cholesterol and egg sphingomyelin at temperatures ranging from 15 to 55 °C. Within experimental accuracy, our results are in good agreement with values from more indepth studies by other groups, conducted at room temperature on DOPE, DOPC, and cholesterol.

Our measurements extend the J_0-list of lipid species and add their temperature dependence.[31] These data will be useful for numerous applications in membrane biophysics.

In the present work we discuss three examples: (i) the monolayer spontaneous curvatures of raft-like lipid mixtures, (ii) line tension of L_o/L_d phases and (iii) evaluation of the line tension during a transition from nanoscopic to microscopic domains. For the studied mixtures of POPC/eggSM/Chol and DOPC/DSPC/Chol, J_0 of the L_o phase was found to be more negative than that of the coexisting L_d phase. DOPC/DPPC/Chol however shows a contrary behavior, with a more positively curved liquid ordered phase due to the positive J_0 of DPPC. This would favor partitioning of barrel-shaped proteins into the L_o phase. Regarding line tension, we found only significant contributions of J_0 for coexisting domains in DOPC/DSPC/Chol. In DOPC/DPPC/Chol and also for the transition from nanoscopic to microscopic domains, γ seems to be dominated by elastic moduli and thickness differences.

Supplementary Material

Refer to Web version on PubMed Central for supplementary material.

Acknowledgments

This work is supported by the Austrian Science Fund FWF, Project no. P24459-B20. The authors thank Karl Lohner, George Khelashvili, Siewert-Jan Marrink, and Ilya Levental for valuable discussions and in particular Daniel Harries for pointing us at the literature explaining delicate differences in spontaneous curvatures.

References

1. Burger KN. Traffic. 2000; 1:605–613. [PubMed: 11208148]
2. Chernomordik LV, Kozlov MM. Nat. Struct. Mol. Biol. 2008; 15:675–683. [PubMed: 18596814]
3. Tamm LK, Crane J, Kiessling V. Curr. Opin. Struct. Biol. 2003; 13:453–466. [PubMed: 12948775]
4. Sheetz MP, Singer SJ. Proc. Natl. Acad. Sci. U. S. A. 1974; 71:4457–4461. [PubMed: 4530994]
5. Evans E. Biophys. J. 1974; 14:923–931. [PubMed: 4429770]
6. Svetina S, Ottova-Leitmannová A, Glaser R. J. Theor. Biol. 1982; 94:13–23. [PubMed: 7078204]
7. Svetina S, Žekš B. Eur. Biophys. J. 1989; 17:101–111. [PubMed: 2766997]
8. Bozic B, Svetina S, Zeks B, Waugh RE. Biophys. J. 1992; 61:963–973. [PubMed: 1581505]
9. Miao L, Seifert U, Wortis M, Döbereiner H-G. Phys. Rev. E: Stat. Phys., Plasmas, Fluids, Relat. Interdiscip. Top. 1994; 49:5389–5407.
10. Seddon, J.; Templer, R. Handbook of biological physics. Vol. 1. North-Holland: 1995. p. 97-160.
11. Cantor RS. J. Phys. Chem. B. 1997; 101:1723–1725.
12. Cantor RS. Chem. Phys. Lipids. 1999; 101:45–56. [PubMed: 10810924]
13. Safran SA. J. Stat. Phys. 1995; 78:1175–1177.
14. Brewster R, Safran SA. Biophys. J. 2010; 98:L21–L23. [PubMed: 20303848]
15. Lundbæk JA, Birn P, Girshman J, Hansen AJ, Andersen OS. Biochemistry. 1996; 35:3825–3830. [PubMed: 8620005]
16. Marsh D. Biophys. J. 2007; 93:3884–3899. [PubMed: 17704167]

17. Boulgaropoulos B, Rappolt M, Sartori B, Amenitsch H, Pabst G. Biophys. J. 2012; 102:2031–2038. [PubMed: 22824266]
18. Pabst G, Boulgaropoulos B, Gander E, Sarangi BR, Amenitsch H, Raghunathan VA, Laggner P. J. Membr. Biol. 2009; 231:125–132. [PubMed: 19882097]
19. Kuzmin PI, Akimov SA, Chizmadzhev YA, Zimmerberg J, Cohen FS. Biophys. J. 2005; 88:1120–1133. [PubMed: 15542550]
20. Akimov SA, Kuzmin PI, Zimmerberg J, Cohen FS. Phys. Rev. E: Stat., Nonlinear, Soft Matter Phys. 2007; 75:011919.
21. Leikin S, Kozlov MM, Fuller NL, Rand RP. Biophys. J. 1996; 71:2623–2632. [PubMed: 8913600]
22. Kozlov, MM. Methods in Membrane Lipids. Springer; 2007. p. 355-366.
23. Kozlov MM, Winterhalter M. J. Phys. II. 1991; 1:1077–1084.
24. Gruner SM, Parsegian VA, Rand RP. Faraday Discuss. 1986; 81:29–37.
25. Tate MW, Gruner SM. Biochemistry. 1989; 28:4245–4253. [PubMed: 2765485]
26. Rand RP, Fuller NL, Gruner SM, Parsegian VA. Biochemistry. 1990; 29:76–87. [PubMed: 2322550]
27. Kozlov MM, Leikin S, Rand RP. Biophys. J. 1994; 67:1603–1611. [PubMed: 7819492]
28. Rand RP, Fuller NL. Biophys. J. 1994; 66:2127–2138. [PubMed: 8075346]
29. Chen Z, Rand RP. Biophys. J. 1997; 73:267–276. [PubMed: 9199791]
30. Chen Z, Rand RP. Biophys. J. 1998; 74:944–952. [PubMed: 9533705]
31. Zimmerberg J, Kozlov MM. Nat. Rev. Mol. Cell Biol. 2005; 7:9–19. [PubMed: 16365634]
32. Kozlov MM, Winterhalter M. J. Phys. II. 1991; 1:1085–1100.
33. Amenitsch H, Rappolt M, Kriechbaum M, Mio H, Laggner P, Bernstorff S. J. Synchrotron Radiat. 1998; 5:506–508. [PubMed: 15263560]
34. Bernstorff S, Amenitsch H, Laggner P. J. Synchrotron Radiat. 1998; 5:1215–1221. [PubMed: 16687824]
35. Huang TC, Toraya H, Blanton TN, Wu Y. J. Appl. Crystallogr. 1993; 26:180–184.
36. Hammersley AP. European Synchrotron Radiation Facility Internal Report ESRF97HA02T. 1997
37. Hammersley AP, Svensson SO, Hanfland M, Fitch AN, Hausermann D. High Pressure Res. 1996; 14:235–248.
38. MATLAB v. 7.12 (R2011a). 2011
39. Hammersley AP, Riekel C. Syn. Rad. News. 1989; 2:24–26.
40. IDL (Interactive Data Language) v. 6.1.
41. IGOR Pro v. 6.2.2.2, 2011.
42. Turner DC, Gruner SM. Biochemistry. 1992; 31:1340–1355. [PubMed: 1736992]
43. Harper PE, Mannock DA, Lewis RN, McElhaney RN, Gruner SM. Biophys. J. 2001; 81:2693–2706. [PubMed: 11606282]
44. Rappolt M, Hodzic A, Sartori B, Ollivon M, Laggner P. Chem. Phys. Lipids. 2008; 154:46–55. [PubMed: 18339315]
45. Alley SH, Ces O, Barahona M, Templer RH. Chem. Phys. Lipids. 2008; 154:64, 67. [PubMed: 18405663]
46. Kučerka N, Tristram-Nagle S, Nagle JF. Biophys. J. 2006; 90:L83–L85. [PubMed: 16617085]
47. Kučerka N, Tristram-Nagle S, Nagle JF. J. Membr. Biol. 2006; 208:193–202. [PubMed: 16604469]
48. Kučerka N, Nagle JF, Sachs JN, Feller SE, Pencer J, Jackson A, Katsaras J. Biophys. J. 2008; 95:2356–2367. [PubMed: 18502796]
49. Kučerka N, Nieh M-P, Katsaras J. Biochim. Biophys. Acta, Biomembr. 2011; 1808:2761–2771.
50. Kirk GL, Gruner SM. J. Phys. 1985; 46:761–769.
51. Vacklin H, Khoo BJ, Madan KH, Seddon JM, Templer RH. Langmuir. 2000; 16:4741–4748.
52. Rappolt M, Hickel A, Bringezu F, Lohner K. Biophys. J. 2003; 84:3111–3122. [PubMed: 12719241]

53. Kooijman EE, Chupin V, Fuller NL, Kozlov MM, de Kruijff B, Burger KNJ, Rand RP. Biochemistry. 2005; 44:2097–2102. [PubMed: 15697235]
54. Safran SA, Pincus P, Andelman D. Science. 1990; 248:354–356. [PubMed: 17784490]
55. Kozlov MM, Helfrich W. Langmuir. 1992; 8:2792–2797.
56. Keller SL, Bezrukov SM, Gruner SM, Tate MW, Vodyanoy I, Parsegian VA. Biophys. J. 1993; 65:23–27. [PubMed: 8369434]
57. Khelashvili G, Harries D, Weinstein H. Biophys. J. 2009; 97:1626–1635. [PubMed: 19751667]
58. May S, Ben-Shaul A. J. Chem. Phys. 1995; 103:3839.
59. Gradzielski M, Langevin D, Sottmann T, Strey R. J. Chem. Phys. 1997; 106:8232–8238.
60. Koynova R, Caffrey M. Biochim. Biophys. Acta, Rev. Biomembr. 1998; 1376:91–145.
61. Uppamoochikkal P, Tristram-Nagle S, Nagle JF. Langmuir. 2010; 26:17363–17368. [PubMed: 20968281]
62. Heberle FA, Wu J, Goh SL, Petruzielo RS, Feigenson GW. Biophys. J. 2010; 99:3309–3318. [PubMed: 21081079]
63. Ionova IV, Livshits VA, Marsh D. Biophys. J. 2012; 102:1856–1865. [PubMed: 22768941]
64. Lingwood D, Simons K. Science. 2010; 327:46–50. [PubMed: 20044567]
65. Smith AK, Freed JH. J. Phys. Chem. B. 2009; 113:3957–3971. [PubMed: 19673072]
66. Ben-Shaul, A. Handbook of biological physics. Vol. 1. North-Holland: 1995. p. 359-401.
67. Schäfer LV, de Jong DH, Holt A, Rzepiela AJ, de Vries AH, Poolman B, Killian JA, Marrink SJ. Proc. Natl. Acad. Sci. U. S. A. 2011; 108:1343–1348. [PubMed: 21205902]
68. Domański J, Marrink SJ, Schäfer LV. Biochim. Biophys. Acta, Biomembr. 2012; 1818:984–994.
69. García-Sáez AJ, Chiantia S, Schwille P. J. Biol. Chem. 2007; 282:33537–33544. [PubMed: 17848582]
70. Lee DW, Min Y, Dhar P, Ramachandran A, Israelachvili JN, Zasadzinski JA. Proc. Natl. Acad. Sci. U. S. A. 2011; 108:9425–9430. [PubMed: 21606329]
71. Helfrich W. Z. Naturforsch., C: J. Biosci. 1973; 693:703.
72. Khelashvili G, Kollmitzer B, Heftberger P, Pabst G, Harries D. J. Chem. Theory Comput. 2013; 9:3866–3871. [PubMed: 24039553]
73. Risselada HJ, Marrink SJ. Proc. Natl. Acad. Sci. U. S. A. 2008; 105:17367–17372. [PubMed: 18987307]
74. Tian A, Johnson C, Wang W, Baumgart T. Phys. Rev. Lett. 2007; 98:208102. [PubMed: 17677743]
75. Esposito C, Tian A, Melamed S, Johnson C, Tee S-Y, Baumgart T. Biophys. J. 2007; 93:3169–3181. [PubMed: 17644560]
76. Honerkamp-Smith AR, Cicuta P, Collins MD, Veatch SL, den Nijs M, Schick M, Keller SL. Biophys. J. 2008; 95:236–246. [PubMed: 18424504]
77. Heberle FA, Petruzielo RS, Pan J, Drazba P, Kučerka N, Standaert RF, Feigenson GW, Katsaras J. J. Am. Chem. Soc. 2013; 135:6853–6859. [PubMed: 23391155]

Europe PMC Funders Author Manuscripts

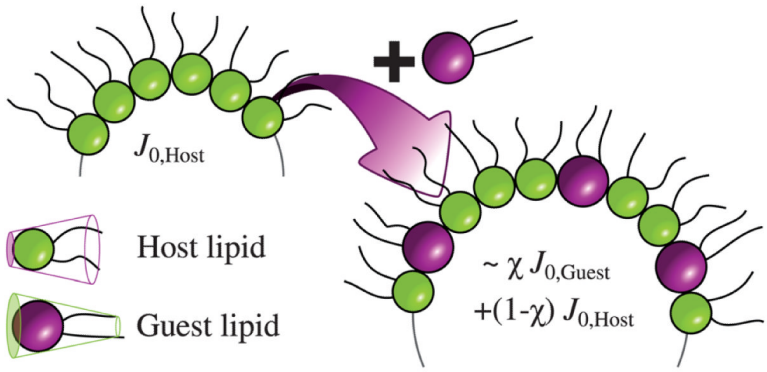

Fig. 1. Guest lipid is incorporated at a concentration χ within the host's template phase.
Note the change of the curvature upon mixing.

Europe PMC Funders Author Manuscripts

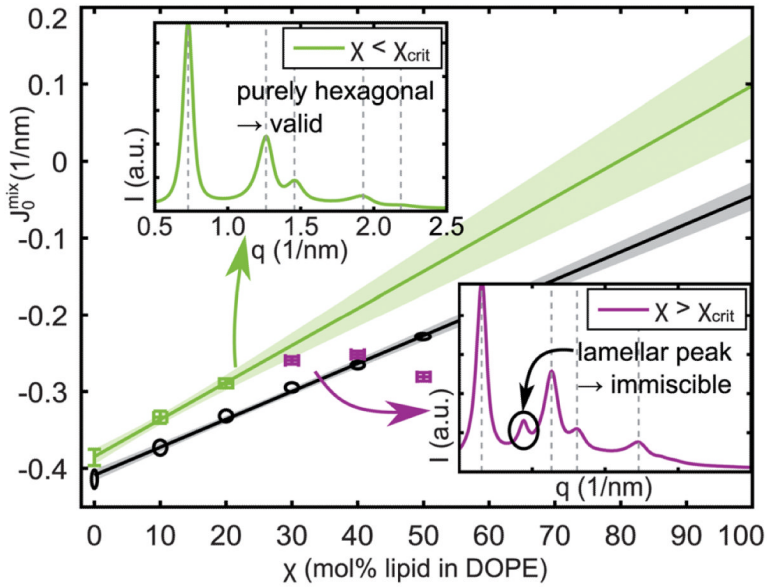

Fig. 2. Determination of J_0^{DPPC} at 25 °C (crosses) and J_0^{POPC} at 45 °C (ellipses) by extrapolation of J_0^{mix} towards χ = 100%.

The insets show X-ray patterns for the last valid (top left) and the first immiscible DPPC data points (bottom right).

Europe PMC Funders Author Manuscripts

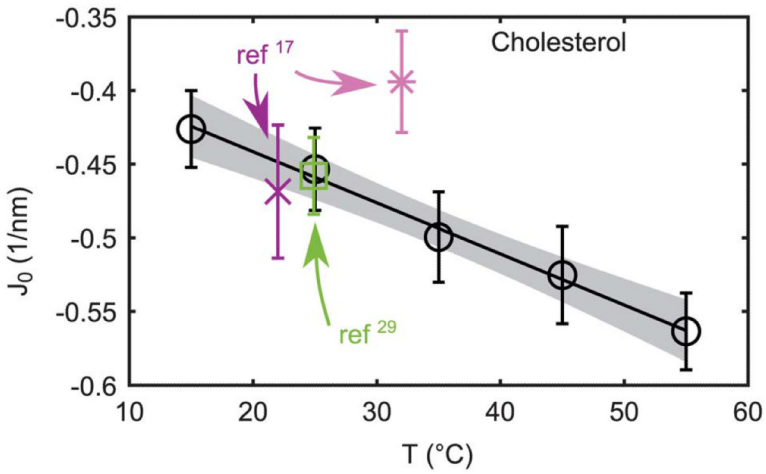

Fig. 3. Comparison between cholesterol spontaneous curvature from the literature (ref. 17 and 29) and new data (circles).

The straight line corresponds to linear fit. Literature data at 32 °C have been determined in a DOPC host matrix, and the other two in DOPE.

Europe PMC Funders Author Manuscripts

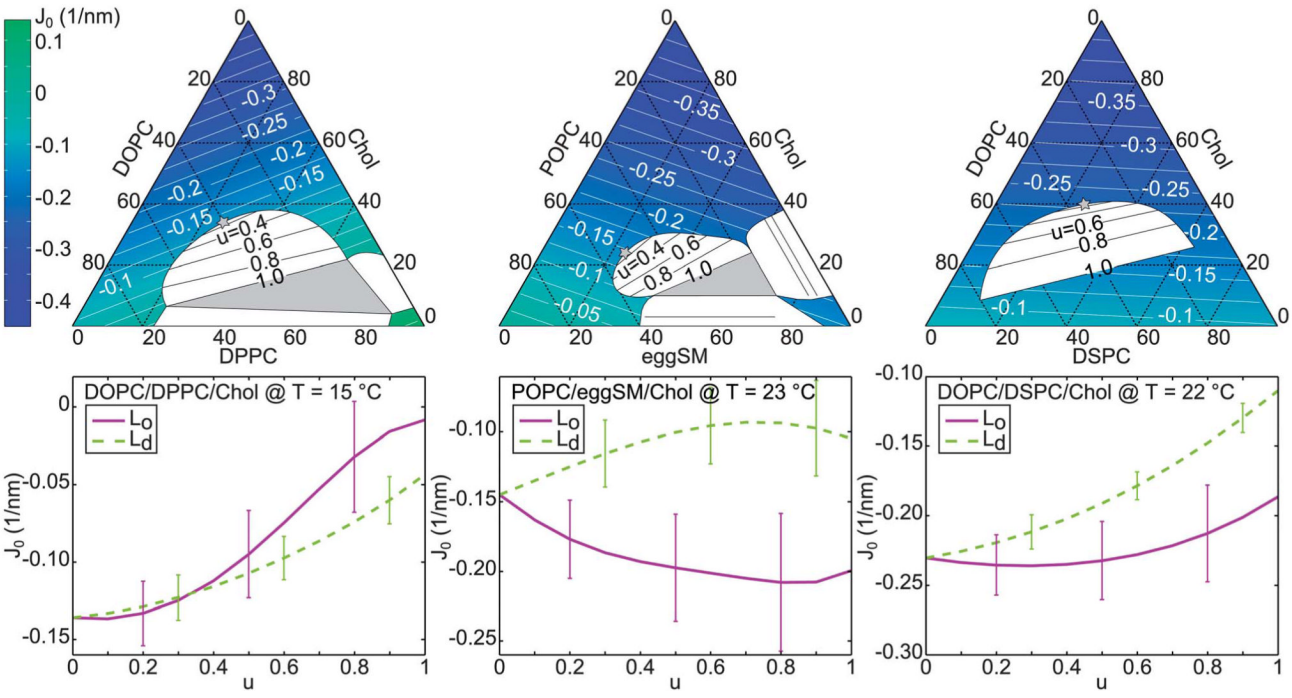

Fig. 4. Spontaneous curvature J_0 (white contours and false-color) for three ternary mixtures within the phase diagrams taken from ref. 61-63.

White segments are two-phase coexistence regions with tielines, gray triangles are three-phase coexistence regions, and gray stars are critical points (top row). The spontaneous curvature J_0 is plotted for coexisting L_o/L_d phases along the boundary of the fluid-fluid phase coexistence regime (bottom row) parameterized by u (see text).

Europe PMC Funders Author Manuscripts

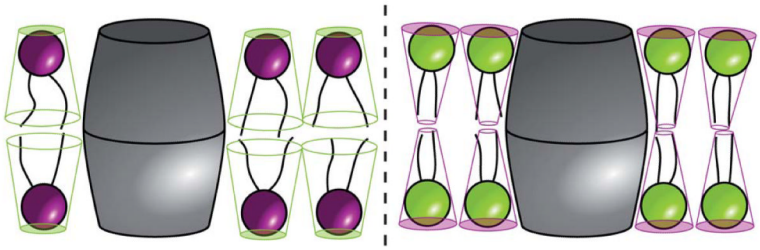

Fig. 5. Barrel shaped transmembrane protein within a bilayer composed of lipids with negative (left) and positive (right) monolayer spontaneous curvatures.
For the latter scenario, the protein shape reduces the packing frustration within the bilayer.

Europe PMC Funders Author Manuscripts

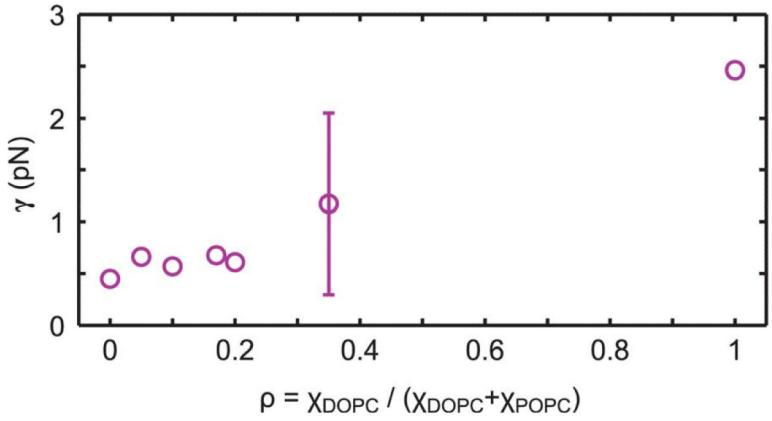

Fig. 6. Calculated line tension γ between L_o and L_d domains in DOPC/POPC/DSPC/Chol.
Uncertainties of all data points are comparable.

Europe PMC Funders Author Manuscripts

Europe PMC Funders Author Manuscripts

Table 1

Parameters describing $J_0(T)$ according to eqn (2) and (3) with T^m = 35 °C, except (*) where T^m = 37 °C

Lipid	$J_0^m \pm \Delta J_0^m$ (1 nm)	$k \pm \Delta k$ (10^{-3}/nm °C)
DOPE	−0.399 ± 0.005	−1.3 ± 0.4
POPE (*)	−0.316 ± 0.007	−2.7 ± 0.7
Chol	−0.494 ± 0.013	−3.5 ± 0.9
DOPC	−0.091 ± 0.008	−1.1 ± 0.6
DPPC	+0.068 ± 0.032	−3.5 ± 2.3
DSPC	−0.100 ± 0.044	−0.2 ± 3.4
POPC	−0.022 ± 0.010	−1.8 ± 0.7
SOPC	−0.010 ± 0.018	−2.2 ± 1.3
eggSM	−0.134 ± 0.072	+1.4 ± 5.1